Cirrus Cloud Microphysical Property Retrieval Using Lidar and Radar Measurements. Part I: Algorithm Description and Comparison with In Situ Data

ZHIEN WANG AND KENNETH SASSEN

Department of Meteorology, University of Utah, Salt Lake City, Utah

(Manuscript received 15 May 2001, in final form 1 September 2001)

ABSTRACT

A retrieval algorithm is described to estimate vertical profiles of cirrus-cloud ice water content (IWC) and general effective size D_{ge} from combined lidar and radar measurements. In the algorithm, the lidar extinction coefficient σ is parameterized as $\sigma = \text{IWC}[a_0 + (a_1/D_{ge})]$ and water equivalent radar reflectivity factor Z_e is parameterized as $Z_e = C'(\text{IWC}/\rho_i)D_{ge}^b$, where a_0, a_1, C', and b are constants based on the assumption of a modified gamma size distribution and hexagonal ice crystals. A comparison of retrieved results from a cirrus-cloud case study with aircraft in situ measurements indicates that the algorithm can provide reliable cirrus cloud microphysical properties. A technique to estimate ice water path and layer-mean D_{ge} is also developed using the optical depth and mean radar reflectivity factor of the cloud layer.

1. Introduction

Cirrus clouds have an important impact on the climate system of our planet (Liou 1986). To improve understanding of the current and predicted future climate, cirrus clouds are regarded as important targets in many research projects (Cox et al. 1987; Stokes and Schwartz 1994). Stephens et al. (1990) have shown that the effects of cirrus clouds depend strongly on cloud microphysical properties, which are poorly known. The microphysical properties of cirrus clouds have been studied with spaceborne (Minnis et al. 1995; Ou et al. 1998; Platt et al. 1999) and ground-based remote sensors (Platt 1979; Sassen et al. 1989; Mastrosov et al. 1992; Intrieri et al. 1993; Mace et al. 1998), in situ aircraft measurements (McFarquhar and Heymsfield 1996), and model simulations (Starr and Cox 1985; Khvorostyanov and Sassen 1998). In situ measurements may provide the most reliable information about cirrus-cloud particles, but the small sample volumes of the probes and the high expense limit aircraft applications in long-term observation programs of cirrus clouds. Although ground-based remote sensing can only provide cloud information at a given location, it can provide high time and space resolution over a long-term period, which are important to improve the physically based cloud parameterizations in GCMs. In addition, ground-based remote sensing studies can help in the development of improved algorithms for space applications using various satellite multispectral radiance methods.

Several promising algorithms have been developed to study cirrus cloud microphysical properties by combining different ground-based remote sensors. Matrosov et al. (1992) estimated layer-average cirrus-cloud parameters from ground-based infrared (IR) radiometer and millimeter-wave radar measurements. Mace et al. (1998) applied this general concept to the particular ensemble of observational platforms at the Department of Energy Atmospheric Radiation Measurement (ARM) Program sites, which was used for routine data analysis at the southern Great Plains (SGP) Cloud and Radiation Test Bed (CART) site.

Matrosov et al. (1994) extended Matrosov et al. (1992) to retrieve ice water content (IWC) and a measure of the characteristic particle size in each radar range gate by applying a statistical technique to deconvolve the measured radial Doppler velocity into mean air motions and particle terminal velocities, often assuming a power relationship between the size of a crystal and its terminal velocity. However, this approach can be used only in the absence of strong convection in clouds. Intrieri et al. (1993) proposed a technique based on carbon dioxide lidar and 35-GHz radar measurements. By assuming the size distribution and shape of ice crystals, this technique retrieves IWC and effective size profiles from the lidar backscattering coefficient β and water equivalent radar reflectivity factor Z_e profiles. To derive vertical profiles of cirrus microphysical properties, other approaches are also tested (Matrosov 1999).

To retrieve cloud microphysical properties correctly in terms of the effect of clouds on the radiation budget,

Corresponding author address: Zhien Wang, Dept. of Meteorology, University of Utah, 135 S 1460 E 819 WBB, Salt Lake City, UT 84112-0110.
E-mail: zwang@met.utah.edu

© 2002 American Meteorological Society

Unauthenticated | Downloaded 05/30/24 12:00 AM UTC

it is vital to include optical (i.e., visible and infrared spectral regions) measurements in the algorithm. Although β and downwelling IR radiance are used in some algorithms (Intrieri et al. 1993; Matrosov et al. 1992), the extinction coefficient σ, derived from the same lidar measurement, was not used. There are two important reasons to use σ rather than β of cirrus clouds derived from lidar measurements. First, backscattering properties of ice crystals are more difficult to model than extinction, especially for visible wavelengths. Yang and Liou (1998) have shown that the phase function at 180° is very sensitive to ice crystal shape, which varies dramatically in cirrus clouds. Second, to get an accurate β profile from lidar measurements, the effect of cloud attenuation still needs to be corrected for; thus a good estimate of the extinction profile is necessary. Thus, more robust algorithms should use the σ profile rather than the β profile (Eberhard et al. 1997).

To retrieve more-reliable cloud macrophysical and microphysical properties, algorithms to combine multiple remote sensors are highly worthwhile. Wang and Sassen (2001b) developed algorithms to study cloud macrophysical properties by combining lidar, cloud radar, and microwave and IR radiometer measurements. In this study, we propose a method that relies on the use of σ from lidar measurements and Z_e from radar measurements to retrieve cirrus microphysical properties. The algorithm description and comparisons with aircraft in situ measurements are presented here. The algorithm is applied to Raman lidar and millimeter cloud radar (MMCR) data collected at the SGP CART site in Oklahoma from November of 1996 to November of 2000, leading to the derivation of basic statistics of cirrus microphysical and radiative properties, as will be discussed in detail in Part II (Wang and Sassen 2001a, manuscript submitted to *J. Atmos. Sci.*).

2. Algorithm description

The objective of this algorithm is to retrieve accurate profiles of IWC and characteristic particle size in cirrus clouds using the σ and Z_e profiles measured by lidar and millimeter-wave radar. Theoretical studies have shown that different characteristic particle sizes have different efficiencies in the parameterization of the radiative properties of cirrus (Ebert and Curry 1992). To take advantage of the parameterization of cirrus-cloud properties developed by Fu (1996), we select the general effective radius D_{ge} as the characteristic size of the particles. From these two parameters, the radiative properties of cirrus can be calculated (Fu 1996; Fu et al. 1998).

The primary assumptions that are needed concern the shape and size distribution of the cirrus particles. Experimental results show that cirrus particles have complex shapes, such as plates, columns, and bullet rosettes, that change over time and space (Sassen et al. 1994; Miloshevich and Heymsfield 1997). This fact means that it is difficult to consider the actual shape of ice particles for a given cloud in an algorithm. Thus, simple shapes are usually used to develop algorithms (Matrosov et al. 1992, 1994; Intrieri et al. 1993; Mace et al. 1998). To use the parameterization of σ with IWC and D_{ge} developed by Fu (1996), we use the same assumption about the shape of ice crystals: randomly oriented hexagons with the aspect ratio D/L (D and L are the width and length of the ice crystal, respectively) given by

$$D/L = \begin{cases} 1.00, & 0 < L \le 30\ \mu\text{m} \\ 0.80, & 30 < L \le 80\ \mu\text{m} \\ 0.50, & 80 < L \le 200\ \mu\text{m} \\ 0.34, & 200 < L \le 500\ \mu\text{m} \\ 0.22, & L > 500\ \mu\text{m}, \end{cases} \tag{1}$$

which roughly corresponds to the observations reported by Auer and Veal (1970).

IWC and D_{ge} are defined in the forms

$$\text{IWC} = \frac{3^{3/2}}{8}\rho_i \int_{L_{\min}}^{L_{\max}} DDLN(L)\, dL \quad \text{and} \tag{2}$$

$$D_{ge} = \frac{\displaystyle\int_{L_{\min}}^{L_{\max}} DDLN(L)\, dL}{\displaystyle\int_{L_{\min}}^{L_{\max}} \left(DL + \frac{\sqrt{3}}{4}D^2\right)N(L)\, dL}, \tag{3}$$

where $N(L)$ is the ice crystal size distribution, $L_{\min}$ and $L_{\max}$ are the minimum and maximum lengths of ice crystals, and ρ_i is the ice crystal density.

Fu (1996) showed that the shortwave σ (m^{-1}) in cirrus can be parameterized as functions of IWC (g m^{-3}) and D_{ge} (μm) as

$$\sigma = \text{IWC}\left(a_0 + \frac{a_1}{D_{ge}}\right), \tag{4}$$

where a_0 and a_1 are coefficients that depend on wavelength. These coefficients are $-2.935\ 99 \times 10^{-4}$ and $2.545\ 40$ for $0.355\ \mu$m (the wavelength used in the Raman lidar), respectively. Fu (1996) also ascertained that the parameterization of σ in terms of D_{ge} does not depend on the assumed ice crystal shape and aspect ratio if using a more general definition for D_{ge}:

$$D_{ge} = \frac{2(3)^{0.5}}{3\rho_i}\frac{\text{IWC}}{A_c}, \tag{5}$$

where A_c is the total cross-sectional area of cloud particles per unit volume.

The gamma distribution or modified gamma distribution is commonly used to represent the size distribution of ice crystals. Here we adopt the modified gamma distribution used by Mace et al. (1998):

$$N(L) = N_X \exp(\alpha)\left(\frac{L}{L_X}\right)^{\alpha} \exp\left(-\frac{L\alpha}{L_X}\right), \tag{6}$$

Unauthenticated | Downloaded 05/30/24 12:00 AM UTC

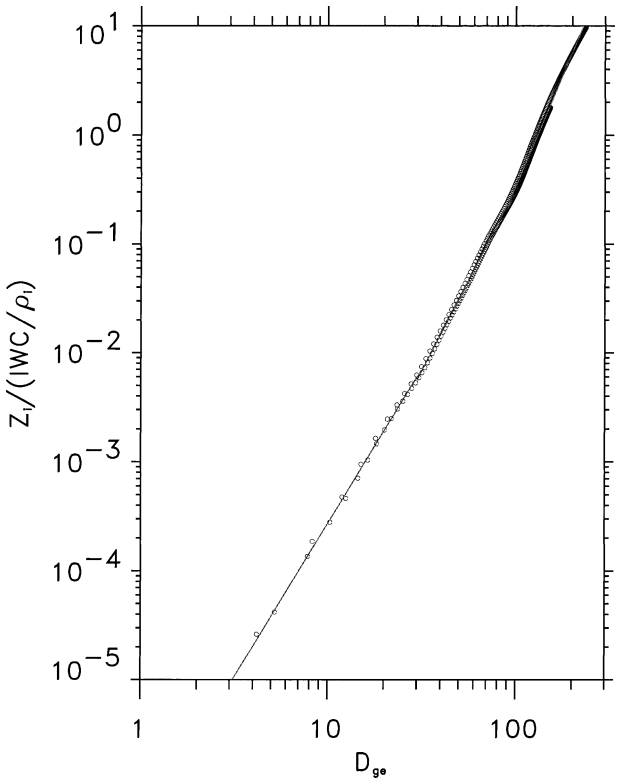

FIG. 1. The quantity Z_i/IWC as a function of D_{ge} calculated with a modified gamma size distribution, where $\alpha = 1$ and 2 and L_X is varied from 2 to 300 μm.

where L_X is the modal length, α is the order, and N_X is the number of particles per unit volume per unit length at the functional maximum.

If we further assume that the Rayleigh approximation is valid (Atlas et al. 1995; Schneider and Stephens 1995) at a radar wavelength of 35 GHz and that the radar reflectivity factor for nonspherical particles can be approximated by its volume equivalent ice sphere, then the Z_i (radar reflectivity factor of volume equivalent solid ice sphere) can be expressed as

$$Z_i = 2^6 \int_{L_{\min}}^{L_{\max}} N(L)\left[\frac{3^{1.5}}{8} D^2 L \Big/ \left(\frac{4}{3}\pi\right)\right]^2 dL. \quad (7)$$

Setting $\alpha = 1$ and 2 (Dowling and Radke 1990), we can calculate Z_i, IWC, and D_{ge} for each size distribution for different L_X. Figure 1 shows Z_i/IWC as a function of D_{ge}, where L_X is changed from 2 to 300 μm. From this figure, we can see that Z_i/IWC has a simple relationship with D_{ge} in a logarithmic scale. Therefore we can parameterize Z_i (mm^6 m^{-3}) with IWC and D_{ge} as

$$Z_i = C\frac{\text{IWC}}{\rho_i} D_{ge}^b, \quad (8)$$

where C and b are constants. To have the best fit with the data, we divide D_{ge} into $D_{ge} < 34.2$ μm, 34.2 μm $\le D_{ge} < 93.9$ μm, and $D_{ge} \ge 93.9$ μm. The line in Fig. 1 is the fitted result, and the corresponding C and b are given in Table 1. We also treated the usual gamma distribution and found that there are no significant differences for the constants in Eq. (8).

TABLE 1. Constants in Eq. (8).

The range of D_{ge} (μm)	C	b
<34.2	$e^{-10.560}$	2.825
34.2–93.9	$e^{-12.509}$	3.377
>93.9	$e^{-15.658}$	4.070

The radar data usually are recorded as Z_e, which refers to a water temperature of 20°C, and can be related to Z_i by

$$Z_e = Z_i(K_i^2/K_w^2), \quad (9)$$

where K_i^2 and K_w^2 are the dielectric constants appropriate for ice and water particles, respectively (Sassen 1987). For 35-GHz radar, $K_i^2 = 0.1768$ and $K_w^2 = 0.93$, and they change negligibly with temperature (Atlas et al. 1995). Combining Eqs. (8) and (9), we have

$$Z_e = C'\frac{\text{IWC}}{\rho_i} D_{ge}^b, \quad (10)$$

where $C' = CK_i^2/K_w^2$.

The IWC and Z_e of ice clouds are both dependent on the ice crystal density, which is not known well. Because we selected the hexagon as the crystal shape rather than a sphere, we simply assume the crystal is solid, that is, $\rho_i = 0.92$ g cm^{-3}, though most ice crystals are not solid and the density changes slightly with size (Heymsfield 1972). If we use the assumptions of spherical particles and the modified gamma or gamma size distribution, effective ρ_i would change with the particle effective size (Atlas et al. 1995; Mace et al. 1998).

Until now, we have parameterized Z_e and σ only in terms of IWC and D_{ge}. It is also straightforward to calculate the downward IR radiance given the IWC and D_{ge} of clouds (Fu et al. 1997, 1998). So, Z_e, σ, and the downward IR radiance are linked together by IWC and D_{ge}.

Besides combining Z_e with the downwelling IR radiance to retrieve layer mean size and IWC or ice water path (IWP, g m^{-2}; Matrosov et al. 1992; Mace et al. 1998), it also can be achieved by simply combining Z_e with cloud visible optical depth τ.

Integrating Eqs. (4) and (10) along the vertical cloud profile results in

$$\tau = \sum_j \sigma(z_j)\Delta z = \sum_j \text{IWC}(z_j)\Delta z\left[a_0 + \frac{a_1}{D_{ge}(z_j)}\right] \quad \text{and} \quad (11)$$

$$\sum_j Z_e(z_j)\Delta z = \sum_j C'[D_{ge}(z_j)]\frac{\text{IWC}(z_j)}{\rho_i}\Delta z \times D_{ge}(z_j)^{b[D_{ge}(z_j)]}, \quad (12)$$

Unauthenticated | Downloaded 05/30/24 12:00 AM UTC

where Δz is the vertical resolution of the profile and z_j is the height of a given gate. To calculate the layer mean size $\overline{D}_{ge}$, we have to neglect the change of D_{ge} with height. With $\overline{D}_{ge}$, Eqs. (13) and (14) are approximated as

$$\tau = \mathrm{IWP}\left(a_0' + \frac{a_1'}{\overline{D}_{ge}}\right) \quad \text{and} \tag{13}$$

$$\overline{Z}_e \Delta H = C_1(\overline{D}_{ge})\left(\frac{K_i^2}{K_w^2 \rho_i}\right)\mathrm{IWP}\overline{D}_{ge}^{\,b'(\overline{D}_{ge})}, \tag{14}$$

where ΔH is the thickness of cloud and $\overline{Z}_e$ is the layer mean Z_e. Here C_1, b', a_0', and a_1' are new constants, which should be different than those in Table 1 and Eq. (4) because of the effects of vertical inhomogeneities in the cloud and nonlinear dependence on D_{ge} in Eqs. (11) and (12). To simplify the problem, we assume $b' = b$, $a_0' = a_0$, and $a_1' = a_1$ and only adjust C for C_1 to take into account the vertical inhomogeneity of cloud particle size; that is, we use C_1 equal to $e^{-12.560}$ and $e^{-14.509}$ and b' equal to 2.825 and 3.377 for $\overline{D}_{ge} \leq 34.2$ μm and $\overline{D}_{ge} > 34.2$ μm, respectively. These adjustments have been tested in two case studies, which show them to work well (Wang 2000).

With the above parameterization, it is straightforward to retrieve IWP and layer-average $\overline{D}_{ge}$ from τ and $\overline{Z}_e$. The τ in the visible region can be inferred from lidar and/or passive measurements.

Combining these equations with other algorithms, we use a strategy to select an algorithm to retrieve cirrus cloud microphysical properties under different situations. If lidar σ and radar Z_e profiles are both available, we can combine these two measurements to obtain IWC and D_{ge} profiles. For optically thin ice clouds, radars are likely to detect only part of the cloud (Wang and Sassen 2001b). In this situation, $\overline{D}_{ge}$ can be estimated from the average σ and Z_e, and the $\overline{D}_{ge}$ and τ can be used to estimate IWP. On the other hand, lidar cannot penetrate optically thick clouds, so it can only provide σ profiles for the lower portion of some ice clouds. In this region, σ can be used to retrieve IWC and D_{ge} at the corresponding altitude with Z_e. For this situation, we can also simply get layer-averaged IWC and D_{ge} by combining IR radiance and Z_e if the cloud infrared absorption depth is smaller than about 3.0 (Matrosov et al. 1992; Mace et al. 1998).

3. Estimation of errors

Uncertainties in IWC and D_{ge} come from two kinds of errors: measurement errors in Z_e and σ and the parameterization errors in Eqs. (4) and (10) due to the assumptions used. The measurement errors in σ result from the effects of signal noise, averaging time, and inversion methods (Klett 1981; Qiu 1988; Ansmann et al. 1992). Even if the SGP CART Raman lidar is used to derive the σ of cirrus clouds, a $\pm 30\%$ error in σ is still possible (Ansmann et al. 1992), especially with daytime measurements for high thin cirrus clouds. For lidars with only an elastic channel, that is, which only receive backscattering at the transmitted wavelengths, we need to use more complicated retrieval algorithms to improve the accuracy of estimated σ (Kovalev 1995; Young 1995).

The measurement errors in Z_e mainly come from the calibration error of the radar system and the effects of noise. A reasonable estimate for the calibration error of most cloud radar systems is 1–3 dBZ. For the SGP CART MMCR, however, the calibration error was reported to be about 1 dBZ, that is, about 25% error in Z_e. The effect of noise depends on the noise level of the system and the averaging time.

The differences between the actual situation and the assumptions involved in formulating the algorithm will also result in errors in Eqs. (4) and (10). Fu (1996) showed that the accuracy of Eq. (4) is very good. However, there is potential error in Eq. (10) due to assuming the shape and size distribution of the ice crystals. To evaluate these assumptions, we make comparisons between the assumed results and the in situ measurements. The in situ measurements used here are about 17 h of 2D cloud probe (2D-C; Particle Measuring Systems, Inc.) data collected by the University of North Dakota Citation aircraft during the SGP CART site intensive observing periods (IOP) of the spring of 1997, autumn of 1997, and spring of 1998. Figure 2 plots Z_i/IWC as a function of D_{ge} calculated from our assumptions (circles, same as shown in Fig. 1) and in situ measurements (black dots). In Fig. 2a, Z_i/IWC from in situ measurements is calculated from the size distributions derived from 2D-C measurements after assuming the same crystal habit used in the algorithm (for more detail on how Z_i, IWC, and D_{ge} are calculated from in situ measurements, see section 4b). On other hand, the in situ Z_i/IWC in Fig. 2b is calculated by using the mass–length relationship of unrimed aggregate plates, bullets, and columns (Locatelli and Hobbs 1974; Brown and Francis 1995). The agreement shown in Fig. 2a indicates that the first- and second-order modified gamma distributions are a good approximation for the actual particle size distributions in cirrus clouds (Dowling and Radke 1990). However, Fig. 2b shows that the crystal habit makes a difference in Eq. (10), and the difference can be up to 50%. Because of the strong variability in crystal habit, the parameterization error in Eq. (10) is also variable for different cloud systems.

The measurement and parameterization errors in our approach affect IWC and D_{ge} in a similar way. To simplify the problem, we only address how the errors in Z_e and σ are transferred to IWC and D_{ge} in this algorithm. If we neglect a_0 in Eq. (4), we can express IWC and D_{ge} simply as functions of Z_e and σ:

Unauthenticated | Downloaded 05/30/24 12:00 AM UTC

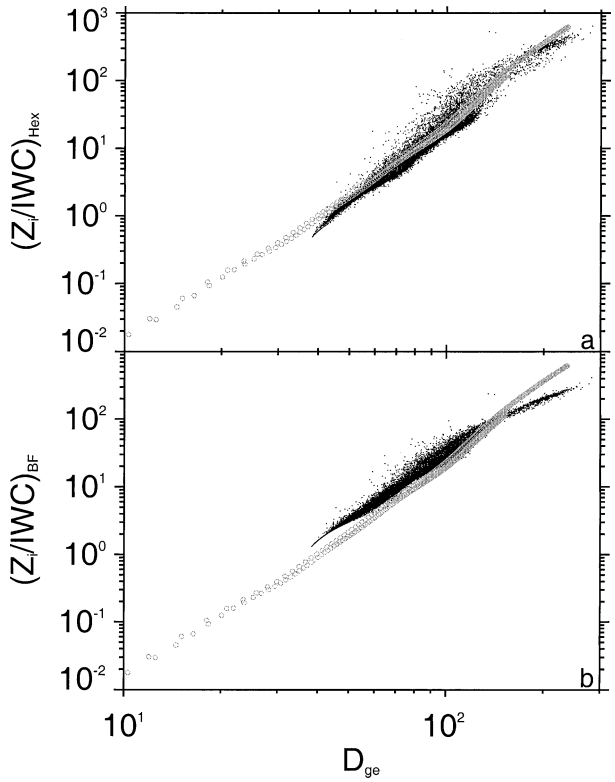

FIG. 2. The quantity Z_i/IWC as a function of D_{ge} calculated from a modified gamma size distribution (circles) and size distributions from 2D-C aircraft measurements (dots), (a) assuming the same habit of ice crystal used in the algorithm and (b) using the mass–length relationship of unrimed aggregate plate, bullets, and columns (Locatelli and Hobbs 1974).

$$D_{ge} = \left(\frac{Z_e}{C'}\right)^{1/(b+1)} \left(\frac{a_1}{\sigma}\right)^{1/(b+1)} \quad \text{and} \qquad (15a)$$

$$\text{IWC} = \left(\frac{Z_e}{C'}\right)^{1/(b+1)} \left(\frac{\sigma}{a_1}\right)^{b/(b+1)}. \qquad (15b)$$

From Eq. (15) we find that Z_e/C' has the same effect on IWC and D_{ge}, but (σ/a_1) affects IWC and D_{ge} in different ways. Table 2 shows how errors are transferred from Z_e and σ to IWC and D_{ge} for $b = 3.37$. We can also see that the error in D_{ge} is smaller than the error in IWC for a given error in Z_e and σ. A 100% error in Z_e/C' causes less than a 20% error in IWC and D_{ge}, which indicates that this algorithm has good tolerance for the measurement errors in Z_e and parameterization error in Eq. (10). The accuracy of IWC is strongly dependent on the accuracy of σ. If there is a $\pm 50\%$ error in σ, the corresponding error in IWC is about $\pm 40\%$. Thus, we can improve the retrieval accuracy of IWC by using accurate σ measurements.

If we retrieve layer-average IWC and D_{ge} from Z_e and τ or downward IR radiance, there is another source of error due to the characteristic vertical inhomogeneity of cirrus cloud microphysical properties (Khvorostyanov and Sassen 1998). However, adjusting the parameterizations to take account of vertical inhomogeneity can reduce this system error.

TABLE 2. The errors in D_{ge} (ΔD_{ge}) and IWC (ΔIWC) in percent, due to error in Z_e and σ.

		$\Delta(Z_e/C')$ (%)			
		−50	0	50	100
		ΔD_{ge} (%)			
$\Delta(\sigma/a_1)$ (%)	−50	−27.2	−14.67	−6.37	0
	0	−14.67	0	9.72	17.18
	50	−6.37	9.72	20.39	28.58
	100	0	17.19	28.58	37.33
		ΔIWC (%)			
$\Delta(a_1/\sigma)$ (%)	−50	−50	−41.4	−35.71	−31.34
	0	−14.67	0	9.72	17.18
	50	16.65	36.7	50	60.2
	100	45.62	70.66	87.25	100

4. Case study of 26 September 1997

The aircraft-supported cirrus case we examine constituted the remains of Hurricane Nora that made landfall in the southwestern United States on 24 September 1997 (Sassen and Mace 2001). The remnants of the cirrus blow-off from the hurricane covered the SGP CART site on 26 September 1997 during a major IOP in which data from several visiting instruments were collected to augment the operational ARM observations. Coordinated in situ data were also collected by the University of North Dakota Citation aircraft from 1800 to 2030 UTC. The CART radiosonde temperature and relative humidity profiles on 26 September 1997 are presented in Fig. 3. The ice saturated relative humidity is plotted by the long-dashed line in Fig. 3a, showing that the moist layer between 8 and 12 km is partly ice supersaturated by 2329 UTC. Figures 4a,b show the University of Utah polarization diversity lidar (PDL; Sassen 1994) relative returned power and the Z_e from the MMCR observed from 1800 to 2100 UTC, as the thickening cirrus layer advected overhead.

Comparison of the lidar and cloud radar data in Fig. 4 illustrates the fundamental differences between lidar and cloud radar. Because of the different wavelengths of lidar and radar, their backscattering coefficients are in proportion to D^2 and D^6, respectively. Although lidar is sensitive enough to detect any kind of cloud in the troposphere, the strong optical attenuation of clouds limits the capability of lidar to penetrate optically thick clouds, as shown in Fig. 4a around 2040 UTC. Cloud radar is considerably more sensitive to large particles than to small particles; therefore, it can fail to detect clouds with small particles. That is the reason why there are holes in the radar display between 1800 and 1910 UTC. For better cloud detection, it is necessary to combine lidar and radar measurements (Wang and Sassen 2001b).

Unauthenticated | Downloaded 05/30/24 12:00 AM UTC

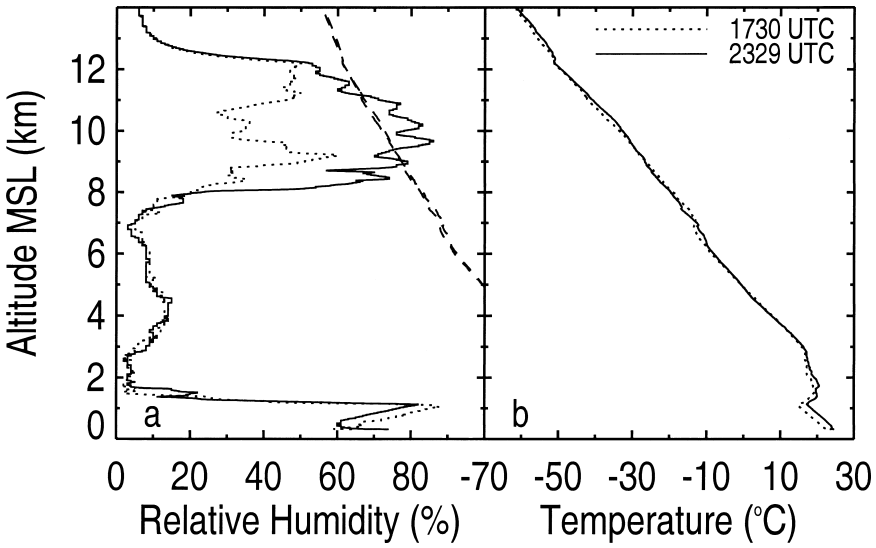

FIG. 3. Radiosonde (a) relative humidity and (b) temperature profiles obtained at the SGP CART site at 1730 and 2329 UTC 26 Sep 1997. The long-dashed lines in (a) represent the ice saturated relative humidity.

a. Retrieved results

The σ of cirrus clouds can be estimated from lidar measurements with different approaches (Klett 1981; Ansmann et al. 1992; Young 1995). The data quality of the CART Raman lidar for this case is too poor to derive σ profiles, but it is possible to estimate τ from its measurements. Then, the estimated τ are used to constrain the retrieval of σ profiles from the PDL measurements. Figures 4c,d show the corresponding height–time displays of retrieved IWC and D_{ge} using σ derived from PDL measurements and MMCR-measured Z_e, in which the cloud microphysical properties can be seen to change with time and increasing cloud thickness. The layer-integrated and mean properties shown in Fig. 5 highlight this point more clearly. Before 1950 UTC, when the cloud is relatively thin, the cirrus cloud is characterized by particles of small size and low IWC. After the transition to thicker cirrus around 2000 UTC, τ is typically greater than 1.5. Although the mean D_{ge} changes with time during this period, the mean IWC is almost constant.

b. Comparisons of cirrus parameters from in situ and ground-based remote measurements

Despite the uncertainties in aircraft measurements and difficulties inherent in sampling the same cloud volume with aircraft and ground-based remote sensors, comparisons between retrieved results with in situ measurements are widely used to judge the performance of algorithms (Mace et al. 1998; Matrosov et al. 1998). The traditional point-to-point comparison, which uses only a very small portion of the data in the analysis, is based on the assumption that they have sampled the same cloud volume. If we assume that in situ and remote sensing measurements can both provide representative samples of this cirrus cloud, then the results should show similar features in a statistical sense, such as in IWC–Z_e and D_{ge}–Z_e relationships. The statistically-based comparison has the advantage that all the in situ data can be used. We will make comparisons using both approaches.

We start from 5-s-average 2D-C data measured by the Citation aircraft. Because the data from the 2D-C probe only contain particles with a maximum length larger than about 50 μm, small crystal information is lacking. There is no simple way to calculate IWC and an effective size from the size distributions measured by the 2D-C because of the complex shapes of ice crystals. The most accurate way to calculate IWC is by particle size spectra, habit percentage, and mass–length relationships dependent on crystal habit (Heymsfield 1977; Locatelli and Hobbs 1974). For most 2D-C data, we lack habit statistics and therefore have to assume the crystal habit and then calculate IWC and Z_e. Brown and Francis (1995) suggested that the mass–length relationship of unrimed aggregate plates, bullets, and columns gives the best estimate of IWC from 2D probe data.

Besides the use of mass–length relationships to convert the measured size information to IWC and Z_e, we can also assume the habit and aspect ratio of an ice crystal to estimate these quantities. As in Kinne et al. (1997), we assume an ice crystal is hexagonal with an aspect ratio from Eq. (1), although we do not employ any particle breakup mechanism. Studies show that IWC derived from the habit-dependent mass–length relationship or the assumption of habit and aspect ratio is only accurate to within a factor of 2 (Heymsfield et al. 1990;

Unauthenticated | Downloaded 05/30/24 12:00 AM UTC

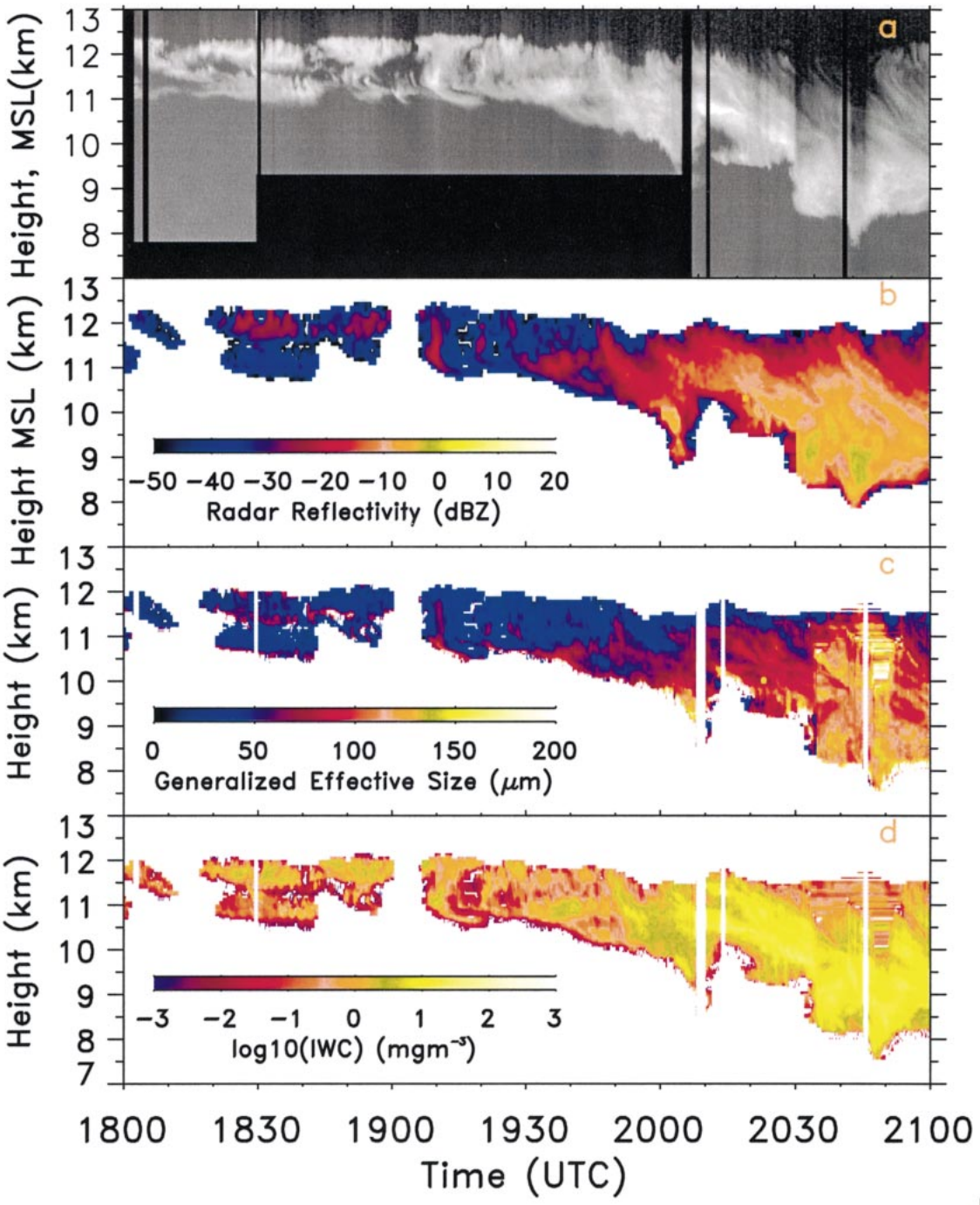

FIG. 4. Height–time displays of observed (a) University of Utah polarization diversity lidar backscatter in arbitrary units (based on a logarithm grayscale) and (b) SGP CART MMCR returns, and the retrieved (c) D_{ge} and (d) IWC at the SGP CART site from 1800 to 2100 UTC on 26 Sep 1997.

Wang 2000). The differences in IWC using various relationships will result in a 1–3 dBZ difference in Z_e. We should be aware of this in the comparison. In the following comparisons, we use Z_e, IWC, and D_{ge} calculated by assuming a hexagonal ice crystal shape with an aspect ratio from Eq. (1).

1) COMPARISONS OF Z_e, *IWC*, AND D_{ge} FROM LIDAR–RADAR AND AIRCRAFT DATA

Figure 6 provides comparisons of Z_e values measured by the SGP CART MMCR with those calculated from aircraft samples. Figures 6a,b show the comparison for

Unauthenticated | Downloaded 05/30/24 12:00 AM UTC

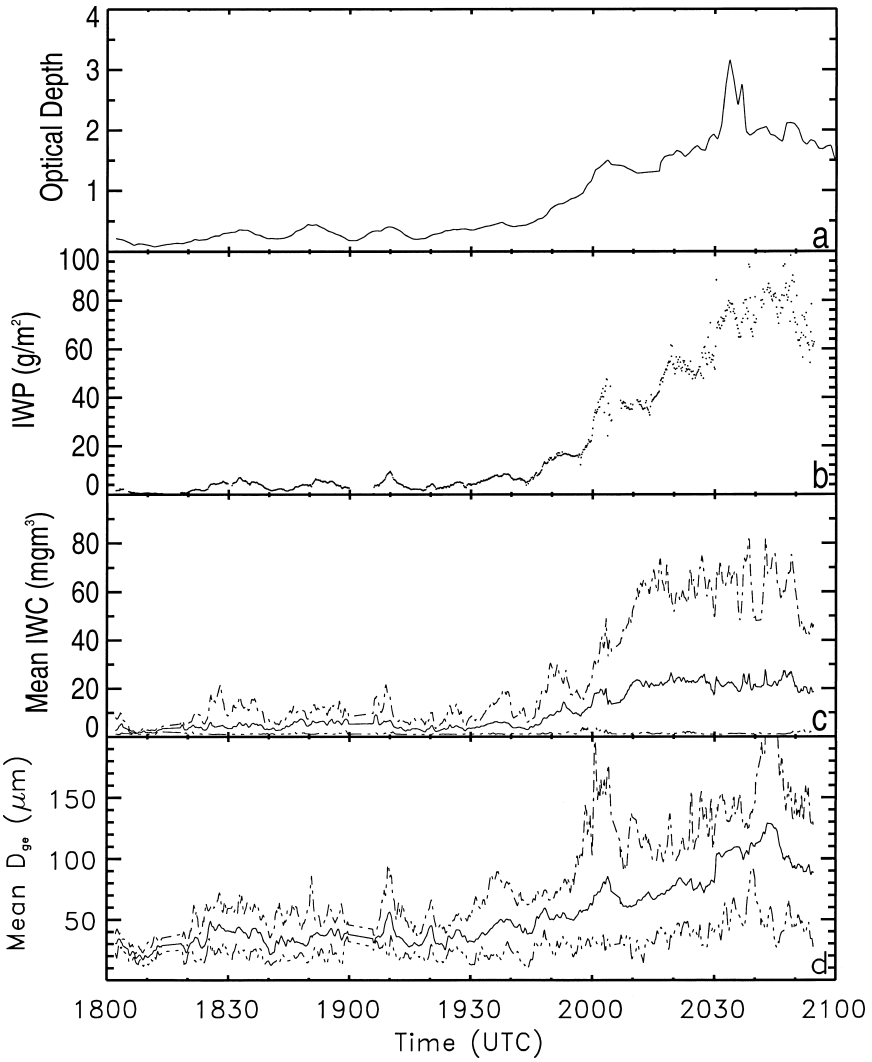

FIG. 5. The layer-integrated and mean properties of the cirrus layer on 26 Sep 1997: (a) optical depth, (b) IWP, (c) mean IWC, and (d) mean D_{ge}. The dashed lines in (c) and (d) are for the minimum and maximum values.

measurements within 3.0 and 1.0 km of the CART site, respectively. The linear correlation coefficient R and the mean difference MD between in situ measurements and lidar–radar retrieval are also shown in the figure. The comparison for measurements obtained within 3.0 km clearly displays more scatter than at 1.0 km. This difference is due mainly to the inhomogeneous nature of cirrus clouds. However, R between measured and calculated Z_e is as high as 92.1% for the measurements within 3.0 km. The mean bias between calculated and measured Z_e is about -1.0 and 0.2 dBZ for the comparisons within 3.0 and 1.0 km, respectively. Considering the uncertainities in calculated Z_e from in situ samples, the possible calibration error in measured Z_e, and the limitations of the comparison due to different sample volumes and instruments based on different principles, we conclude that the agreement between measured and calculated radar reflectivities is good.

The comparisons between IWC retrieved from lidar–radar measurements and calculated from aircraft samples are shown in Figs 7a,b, again providing data between measurements within 3.0 and 1.0 km of the CART site, respectively. The R between retrieved and calculated IWC is only 67.7% for the measurements within 3.0 km but is 98.4% for the measurements within 1.0 km. The MD of log(IWC) between calculated and retrieved values is very small, or about -0.08 and -0.09 for measurements within 3.0 and 1.0 km, respectively. In other words, the retrieved IWC is about 20% higher than that inferred from in situ measurements.

As mentioned above, the uncertainty in IWC calculated from in situ samples can be up to a factor of 2.

Unauthenticated | Downloaded 05/30/24 12:00 AM UTC

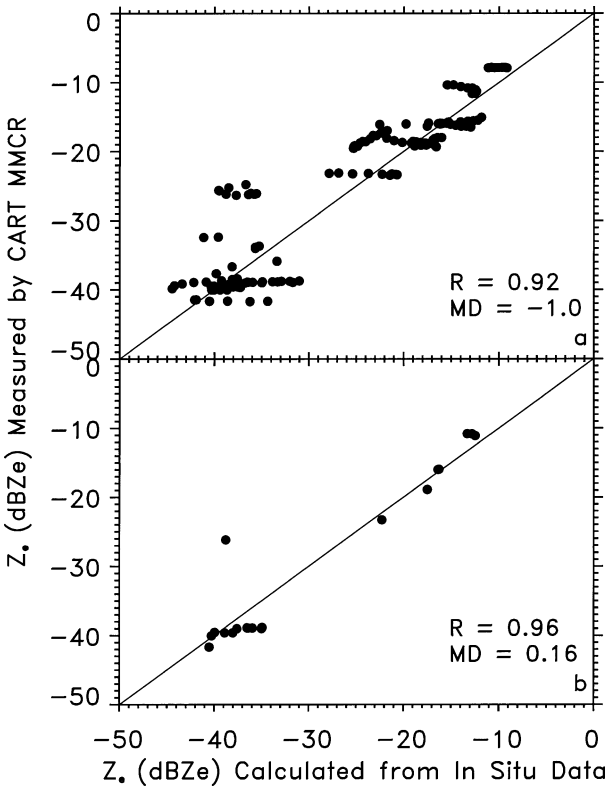

FIG. 6. Comparisons of Z_e values measured by MMCR with those calculated from aircraft 2D-C data using the assumption of hexagonal ice crystal with an aspect ratio from Eq. (1): (a) measurements within 3.0 km and (b) measurements within 1.0 km from the SGP CART site. The linear correlation coefficient and the mean difference between in situ measurements and lidar–radar retrievals are given.

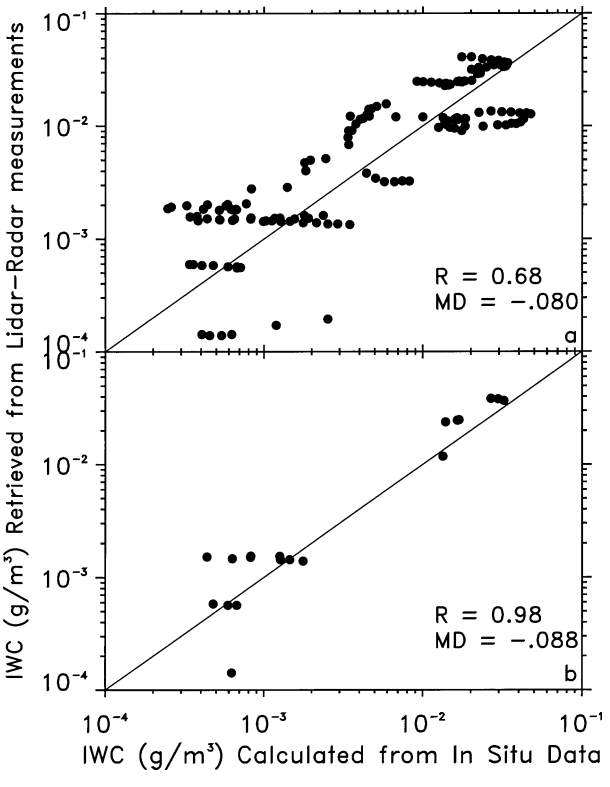

FIG. 7. Comparisons of IWC retrieved from lidar–radar measurements and calculated from aircraft 2D-C data, as in Fig. 6.

If we use estimated IWC with the mass–length relationship for unrimed aggregate plates, bullets, and columns, the inferred IWC will be higher than that retrieved. On the other hand, we lack size information for small ice particles, which could have a significant contribution to IWC. The retrieved IWC also has about a 10%–40% error. From Fig. 7, we can see that the variation in IWC is up to 3 orders of magnitude. Given such a large dynamic range in IWC and given the uncertainties in both measurements, the overall agreement between retrieved and calculated IWC can be considered to be good.

Figure 8 presents the comparisons of lidar–radar and aircraft-derived D_{ge}. The R is about 85%, and MD is about -0.66 and 5.9 μm for measurements within 3.0 and 1.0 km, respectively. Note that there is no large difference in R between the comparisons for measurements within 3.0 and 1.0 km. For the retrieved D_{ge} smaller than 45 μm, the in situ–derived D_{ge} is always larger than the retrieved D_{ge}, which is mainly due to the 2D-C probe lacking small crystal size information. The complex shapes of ice crystals make it difficult to estimate any kind of characteristic size accurately, so different approaches usually provide different results. Assuming 20% random errors in both measurements, we would satisfy the agreement between retrieved and calculated D_{ge}. Taking into account the uncertainties in both 2D-C and ground-based remote sensing measurements and the limitations of point-to-point comparisons, the overall agreement is reasonable.

2) Comparisons of average IWC–Z_e and D_{ge}–Z_e relationships from lidar–radar and aircraft data

To use the aircraft data more fully, we make comparisons based on average IWC–Z_e and D_{ge}–Z_e relationships in Fig. 9. Figure 9a compares the scatterplots of IWC retrieved from lidar–radar measurements versus measured Z_e. The IWC-versus-Z_e data points from aircraft data are also plotted as gray circles. The mean values of log(IWC) versus Z_e are given in Fig. 9b, where the vertical lines indicate standard deviations. From Fig. 9b, we can see that the derived IWC–Z_e relationships are similar when Z_e is between -30 and -10 dBZ. The average difference in mean log(IWC) is less than 0.1 in this Z_e range. The standard deviations of log(IWC) from aircraft samples are smaller than those of the lidar–radar data because the in situ sample volumes are much smaller. When Z_e is less than -30 dBZ, the difference increases because the 2D-C probe data miss information

Unauthenticated | Downloaded 05/30/24 12:00 AM UTC

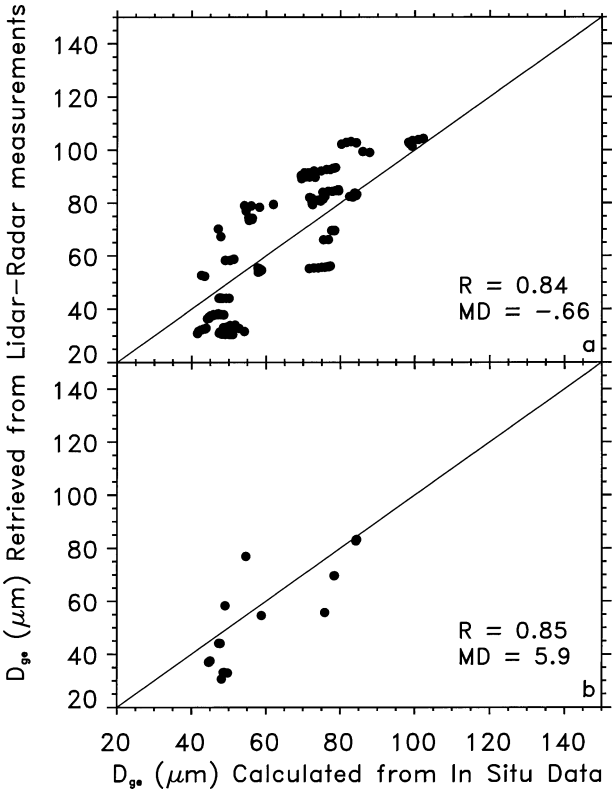

FIG. 8. Comparisons of D_{ge} retrieved from lidar–radar measurements and calculated from aircraft 2D-C data, as in Fig. 6.

concerning small ice crystals, which can be expected to have a larger contribution to IWC than to Z_e.

Similar comparisons for D_{ge}–Z_e relationships are shown in Figs. 9c, d. The average size difference in mean D_{ge} is about 5 μm when Z_e lies within -30 and -10 dBZ. When Z_e is less than -30 dBZ, the inferred aircraft D_{ge} is much larger than the mean D_{ge} from lidar–radar measurements, which is also mainly due to the underestimation of small ice crystals in the aircraft data. From the above discussion, we conclude that the statistical comparisons based on IWC–Z_e and D_{ge}–Z_e relationships also show good agreement between lidar–radar and aircraft measurements, indicating that our lidar–radar algorithm [Eqs. (4) and (10)] provides reliable information about cirrus-cloud contents.

5. Conclusions

A retrieval algorithm is presented to estimate cirrus cloud IWC and D_{ge} profiles from combined lidar and radar measurements. In the algorithm, σ and Z_e are parameterized as simple functions of IWC and D_{ge}; thus the retrieval of IWC and D_{ge} from measured σ and Z_e is straightforward. The case-study results and comparisons with aircraft in situ data indicate that this algorithm can provide reliable cirrus cloud microphysical properties. A technique to estimate IWP and layer mean D_{ge} is also developed using τ and the mean Z_e of the cloud layer. Results from these new algorithms can be used to study cloud radiative forcing and vertical and horizontal cloud inhomogeneity. The algorithms have been developed based on several assumptions and thus can be improved with more advanced knowledge concerning the size distributions, ice crystal shape and bulk density, and backscattering properties of complex ice crystals at lidar and radar wavelengths.

A potential drawback to this approach is that millimeter-wave radars, depending on their sensitivity, may fail to detect those optically thin portions of cirrus clouds that contain small particles, especially near cloud top, and lidar cannot penetrate optically thick cirrus clouds. We have suggested ways to overcome this deficiency to estimate data quantities in such regions. However, because experimental and model results have shown that the size of cirrus-cloud particles varies characteristically with height (Sassen et al. 1989; Khvorostyanov and Sassen 1998), it may be possible to estimate an average particle size for the upper portion of the cloud from the size information derived in the lower cloud. Then, an IWC profile can be retrieved in the upper cloud region from the available σ or Z_e and the estimated particle size.

The algorithms developed in this study have the potential to improve our capability to study cirrus clouds. As an example, the algorithm has been applied to Raman lidar and MMCR data collected at the SGP CART site in Oklahoma during November of 1996 to November of 2000, and basic statistics of cirrus microphysical and radiative properties will be derived and presented in Part II. Applying these algorithms to additional datasets from the ARM CART sites will provide a valuable database to study cirrus cloud microphysical and radiative properties and, finally, to find an optimal way to parameterize cirrus clouds in GCMs. However, we recognize that lidar–radar algorithms cannot retrieve cirrus microphysical properties in the presence of low- or midlevel clouds, which typically block lidar observation from the ground.

The planned CloudSat and Earth System Science Pathfinder (ESSP-3) satellite deployments will carry a millimeter-wave radar and lidar to study the vertical profile of clouds from Earth orbit. Although considerable revisions to our algorithms will be required in view of the different remote sensor specifications and operational capabilities, we intend to develop an approach to maximize the information content of active remote sensing observation from satellites based on our ground-based algorithm research.

Acknowledgments. Algorithm development has been supported by the Office of Biological and Environment Research of the U.S. Department of Energy (under Grant DEFG0394ER61747) as part of the Atmospheric Radiation Measurement Program and from NASA Grant NAS7-1407 from the CloudSat program. We thank M.

Unauthenticated | Downloaded 05/30/24 12:00 AM UTC

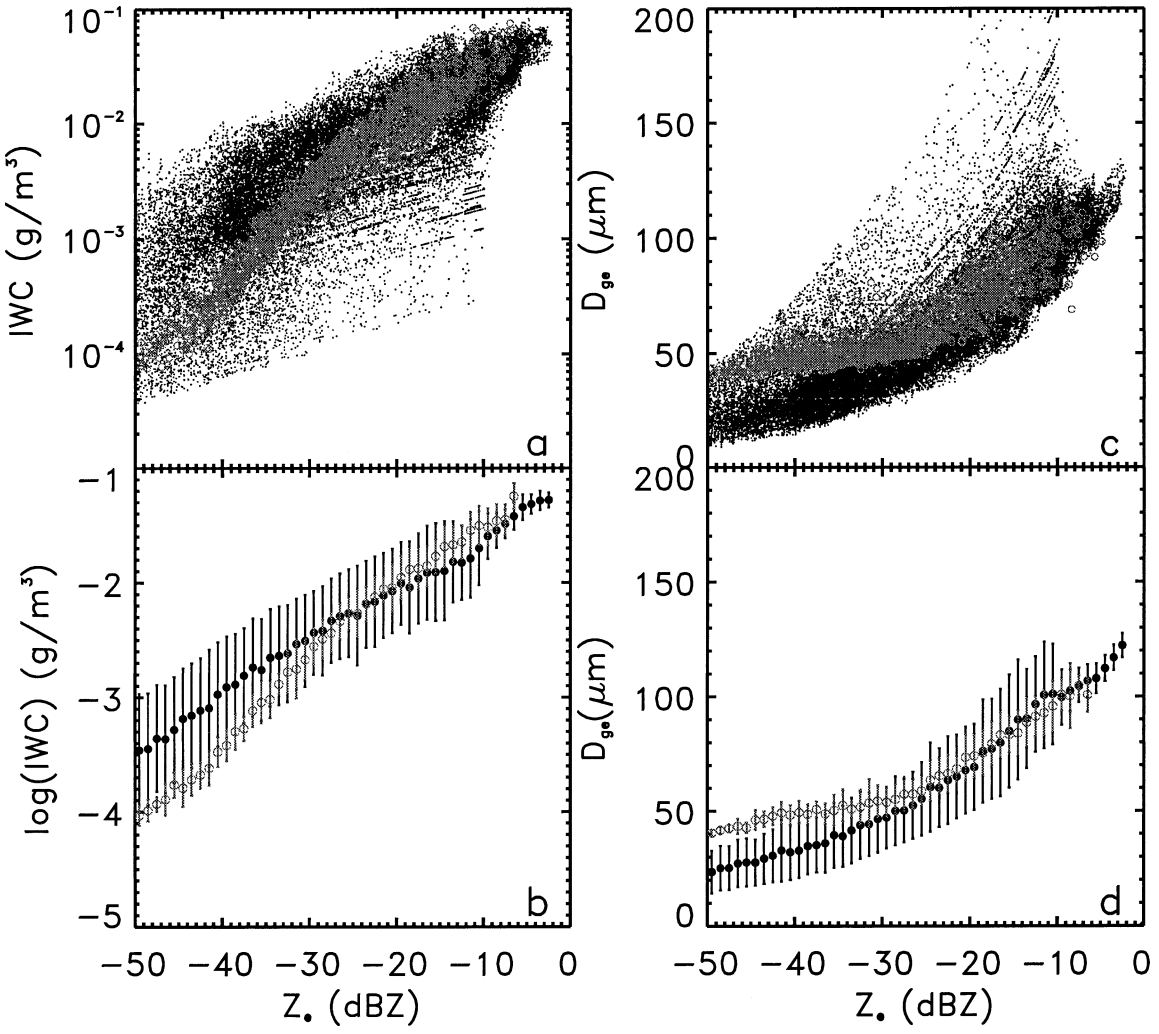

FIG. 9. Comparisons of IWC–Z_e and D_{ge}–Z_e relationships between aircraft 2D-C data (in gray circles) and ground-based remote sensing (black): (a) scatterplot of IWC vs Z_e, (b) mean of log(IWC) (with std dev) vs Z_e, (c) scatterplot of D_{ge} vs Z_e, and (d) mean D_{ge} (with std dev) vs Z_e.

R. Poellot for providing the in situ data. We thank the anonymous reviewers for their comments.

REFERENCES

Ansmann, A., U. Wandinger, M. Riebesell, C. Weitkamp, and W. Michaelis, 1992: Independent measurement of extinction and backscatter profiles in cirrus clouds by using a combined Raman elastic–backscatter lidar. *Appl. Opt.,* **31,** 7113–7131.

Atlas, D., S. Y. Matrosov, A. J. Heymsfield, M. D. Chou, and D. B. Wolff, 1995: Radar and radiation properties of ice clouds. *J. Appl. Meteor.,* **34,** 2329–2345.

Auer, A. H., Jr., and D. L. Veal, 1970: The dimension of ice crystals in natural clouds. *J. Atmos. Sci.,* **27,** 919–926.

Brown, P. R. A., and P. N. Francis, 1995: Improved measurements of the ice water content in cirrus using a total-water probe. *J. Atmos. Oceanic Technol.,* **12,** 410–414.

Cox, S. K., D. S. McDougal, D. A. Randall, and R. A. Schiffer, 1987: FIRE—The First ISCCP Regional Experiment. *Bull. Amer. Meteor. Soc.,* **68,** 114–118.

Dowling, D. R., and L. F. Radke, 1990: A summary of the physical properties of cirrus clouds. *J. Appl. Meteor.,* **29,** 970–978.

Eberhard, W. L., S. Y. Matrosov, A. S. Frisch, and J. M. Intrieri, 1997: Microphysical retrievals from simultaneous radar and optical or microwave measurements. *Proc. WMO Workshop on Cloud Observations,* Mexico City, Mexico, WMO, 248–254.

Ebert, E. E., and J. A. Curry, 1992: A parameterization of ice cloud optical properties for climate models. *J. Geophys. Res.,* **97,** 3831–3836.

Fu, Q., 1996: An accurate parameterization of the solar radiative properties of cirrus clouds for climate models. *J. Climate,* **9,** 2058–2082.

——, K. N. Liou, M. C. Cribb, T. P. Charlock, and A. Grossman, 1997: Multiple scattering parameterization in thermal infrared radiative transfer. *J. Atmos. Sci.,* **54,** 2799–2812.

——, P. Yang, and W. B. Sun, 1998: An accurate parameterization of the infrared radiative properties of cirrus clouds for climate models. *J. Climate,* **11,** 2223–2237.

Heymsfield, A. J., 1972: Ice crystal terminal velocities. *J. Atmos. Sci.,* **29,** 1348–1357.

——, 1977: Precipitation development in stratiform ice clouds: A microphysical and dynamical study. *J. Atmos. Sci.,* **34,** 367–381.

——, K. M. Miller, and J. D. Spinhirne, 1990: The 27–28 October 1986 FIRE IFO cirrus case study: Cloud microstructure. *Mon. Wea. Rev.,* **118,** 2313–2328.

Unauthenticated | Downloaded 05/30/24 12:00 AM UTC

Intrieri, J. M., G. L. Stephens, W. Eberhard, and T. Uttal, 1993: A method for determining cirrus cloud particle sizes using a lidar and radar backscatter technique. *J. Appl. Meteor.,* **32,** 1074–1082.

Khvorostyanov, V. I., and K. Sassen, 1998: Cirrus cloud simulation using explicit microphysics and radiation. Part II: microphysics, vapor and ice mass budgets, and optical and radiative properties. *J. Atmos. Sci.,* **55,** 1822–1845.

Kinne, S., and Coauthors, 1997: Cirrus cloud radiative and microphysical properties from ground observations and in situ measurements during FIRE 1991 and their application to exhibit problems in cirrus solar radiative transfer modeling. *J. Atmos. Sci.,* **54,** 2320–2344.

Klett, J. D., 1981: Stable analytical inversion solution for processing lidar returns. *Appl. Opt.,* **20,** 211–220.

Kovalev, V. A., 1995: Sensitivity of the lidar solution to errors of the aerosol backscatter-to-extinction ratio: Influence of a monotonic change in the aerosol extinction coefficient. *Appl. Opt.,* **34,** 3457–3462.

Liou, K. N., 1986: Influence of cirrus cloud on weather and climate processes: A global perspective. *Mon. Wea. Rev.,* **114,** 1167–1199.

Locatelli, J. D., and P. V. Hobbs, 1974: Fall speeds and masses of solid precipitation particles. *J. Geophys. Res.,* **79,** 2185–2197.

Mace, G. G., T. A. Ackerman, P. Minnis, and D. F. Young, 1998: Cirrus layer microphysical properties derived from surface-based millimeter radar and infrared interferometer data. *J. Geophys. Res.,* **103,** 23 027–23 216.

Matrosov, S. Y., 1999: Retrieval of vertical profiles of ice cloud microphysics from radar and IR measurements using tuned regressions between reflectivity and cloud parameters. *J. Geophys. Res.,* **104,** 16 741–16 753.

——, T. Uttal, J. B. Snider, and R. A. Kropfli, 1992: Estimation of ice cloud parameters from ground-based infrared radiometer and radar measurements. *J. Geophys. Res.,* **97,** 11 567–11 574.

——, B. W. Orr, R. A. Kropfli, and J. B. Snider, 1994: Retrieval of vertical profiles of cirrus cloud microphysical parameters from Doppler radar and infrared radiometer measurements. *J. Appl. Meteor.,* **33,** 617–626.

——, A. J. Heymsfield, R. A. Kropfli, B. E. Martner, R. F. Reinking, J. B. Snider, P. Piironen, and E. W. Eloranta, 1998: Comparisons of ice cloud parameters obtained by combined remote sensor retrievals and direct methods. *J. Atmos. Oceanic Technol.,* **15,** 184–196.

McFarquhar, G. M., and A. J. Heymsfield, 1996: Microphysical characteristics of three anvils sampled during the Central Equatorial Pacific Experiment (CEPEX). *J. Atmos. Sci.,* **53,** 2401–2423.

Miloshevich, L. M., and A. J. Heymsfield, 1997: A balloon-borne continuous cloud particle replicator for measuring vertical profiles of cloud microphysical properties: Instrument design, performance, and collection efficiency analysis. *J. Atmos. Oceanic Technol.,* **14,** 753–768.

Minnis, P., and Coauthors, 1995: Cloud optical property retrieval (subsystem 4.3). *Clouds and the Earth's Radiant Energy System (CERES) Algorithm Theoretical Basis Document: Cloud Analyses and Radiance Inversions (Subsystem 4)*, Vol. 3, NASA Tech. Rep. RP 1376, 135–176.

Ou, S. C., K. N. Liou, and T. R. Caudill, 1998: Remote sounding of multilayer cirrus cloud systems using AVHRR data collected during FIRE-II-IFO. *J. Appl. Meteor.,* **37,** 241–254.

Platt, C. M. R., 1979: Remote sounding of high clouds: I. Calculation of visible and infrared optical properties from lidar and radiometer measurements. *J. Appl. Meteor.,* **18,** 1130–1143.

——, D. M. Winker, M. A. Vaughan, and S. D. Miller, 1999: Backscatter-to-extinction ratios in the top layer of tropical mesoscale convective systems and in isolated cirrus from LITE observations. *J. Appl. Meteor.,* **38,** 1330–1345.

Qiu, Q., 1988: Sensitivity of lidar equation solution to boundary values and determination of the values. *Adv. Atmos. Sci.,* **5,** 229–241.

Sassen, K., 1987: Ice cloud content from radar reflectivity. *J. Climate Appl. Meteor.,* **26,** 1050–1053.

——, 1994: Advances in polarization diversity lidar for cloud remote sensing. *Proc. IEEE,* **82,** 1907–1914.

——, and G. G. Mace, 2001: Ground-based remote sensing of cirrus clouds. *Cirrus,* D. Lynch, et al., Eds., Oxford University Press, 168–196.

——, D. O'C. Starr, and T. Uttal, 1989: Mesoscale and microscale structure of cirrus clouds: Three case studies. *J. Atmos. Sci.,* **46,** 371–386.

——, N. C. Knight, Y. Takano, and A. J. Heymsfield, 1994: Effects of ice-crystal structure on halo formation: Cirrus cloud experimental and ray-tracing modeling studies. *Appl. Opt.,* **33,** 4590–4601.

Schneider, T. L., and G. L. Stephens, 1995: Theoretical aspects of modeling backscattering by cirrus particles at millimeter wavelengths. *J. Atmos. Sci.,* **52,** 4367–4385.

Starr, D. O'C., and S. K. Cox, 1985: Cirrus clouds. Part II: Numerical experiments on the formation and maintenance of cirrus. *J. Atmos. Sci.,* **42,** 2682–2694.

Stephens, G. L., S. Tsay, P. W. Stackhouse, and P. J. Flatau, 1990: The relevance of the microphysical and radiative properties of cirrus clouds to climate and climatic feedback. *J. Atmos. Sci.,* **47,** 1742–1753.

Stokes, G. M., and S. E. Schwartz, 1994: The Atmospheric Radiation Measurement (ARM) Program: Programmatic background and design of the Cloud and Radiation Test Bed. *Bull. Amer. Meteor. Soc.,* **75,** 1201–1221.

Wang, Z., 2000: Cloud property retrieval using combined ground-based remote sensors. Ph.D. dissertation, Dept. of Meteorology, University of Utah, 184 pp.

——, and K. Sassen, 2001a: Cirrus cloud microphysical property retrieval using lidar and radar measurements. Part II: Midlatitude cirrus microphysical and radiative properties. *J. Atmos. Sci.,* submitted.

——, and ——, 2001b: Cloud type and macrophysical property retrieval using multiple remote sensors. *J. Appl. Meteor.,* **40,** 1665–1682.

Yang, P., and K. N. Liou, 1998: Single-scattering properties of complex ice crystals in terrestrial atmosphere. *Contrib. Atmos. Phys.,* **71,** 223–248.

Young, S. A., 1995: Analysis of lidar backscatter profiles in optically thin clouds. *Appl. Opt.,* **34,** 7019–7031.

Unauthenticated | Downloaded 05/30/24 12:00 AM UTC